Interaction of displacement amplitude and frequency effects in fretting wear of a high strength steel: impact on debris bed formation and subsurface damage

A.M. Kirk, W. Sun, C.J. Bennett, P.H. Shipway

Faculty of Engineering, University of Nottingham, UK

Abstract

In previous work, fretting frequency has been observed to have a significant impact not only on wear rates, but also on the nature of fretting debris and the development of subsurface damage; however, while the "frequency effect" has been shown in some cases to be affected by the amplitude of the displacement, the mechanism of the interrelationship is not well understood. The present work presents new insights into the frequency effect by investigating the impact of displacement amplitude on fretting wear over a range of frequencies. Experiments were conducted using like-on-like high strength steel pairs in a cylinder-on-flat configuration. Irrespective of test conditions, the ejected debris was almost entirely made up of iron oxide with only a small fraction of metallic material. It was observed that as displacement amplitude was increased, the debris beds became sparser with a higher proportion of exposed metallic surface in the scar, with extensive deformation and cracking being observed in the metallic material; in contrast, at lower displacement amplitudes, sufficient oxygen is available to continually form oxide throughout the contact, which significantly reduces the development of such sub-surface damage.

It is proposed that damage and wear in fretting is controlled by (i) oxygen ingress to the contact; (ii) oxide debris formation; (iii) debris expulsion from the contact. Wear and damage in fretting is controlled by whichever of these processes has the lowest rate under the test conditions being employed, which is then termed the rate-determining process.

1 Introduction

Fretting wear is a process of material removal and surface degradation resulting from small amplitude relative oscillatory motion in a contact between loaded components and is found to occur in many industrial contexts. In fretting, the displacements are small relative to the overall contact size which means that the debris remains in the contact for a considerable time; during this time, the debris plays a significant role in determining the operative physical processes of degradation. The rate of wear in fretting is commonly described as the change in wear volume with distance slid or as the change in wear volume with frictional energy dissipated [1]; the more commonly used energy-based wear rate will be used in this work. An approach to fretting wear which describes the rate of wear as being controlled by the ejection of detached debris particles from the contact (rather than solely by their initial detachment from the surfaces of the bodies in contact) was formalised by Godet and co-workers, who termed it the third body approach [2–6]. As part of this, they argued that oxide debris retained in the contact can act as a solid lubricant and thus protect the first bodies from more damaging metal-to-metal (first-body) contact.

As well as its role in limiting metal-metal contact in fretting (and the resulting sub-surface damage), it has been argued that oxide debris formed in fretting may also act as an abrasive (due to its high hardness relative to that of the metal bodies in contact) [4,7–9]. Such complexity regarding the behaviour of debris particles in fretting (such as the balance between its protective and antagonistic

effects) is a factor that hinders the development of accurate predictive models incorporating the role of debris in fretting [10].

It has been observed that when an oxide debris layer is not present to separate the first-body metallic surfaces in fretting, high levels of adhesive transfer along with extensive sub-surface deformation and damage in the bulk metal can occur [11–15]; this sub-surface deformation is typically referred to as the tribologically transformed structure (TTS) [16]. However, it is the expulsion of oxide-based debris that results in wear and so in situations where oxide debris is not readily formed, it results (apparently paradoxically) in both a reduction in wear and, at the same time, an increase in severe sub-surface damage [13–15]. Previous work by the current authors [14] investigating the effect of frequency on a high strength steel found that (for a given set of test parameters) as frequency was increased from 20 Hz to 200 Hz, scars became more metallic and severely damaged with regions of metallic transfer between the contacting bodies being observed towards the centre of contacts where oxygen access is most restricted. A significant reduction in wear rate was also observed as frequency was increased; such reductions in wear rate with increasing frequency have been widely reported in the literature [13,15,17–23].

Warmuth et al. [20] observed that the changes in wear rates and mechanisms in fretting of steel pairs resulting from changes in frequency were heavily influenced by the physical size of the contact, attributing the effect to the exclusion of oxygen from the interface; as part of this, debris that remained within wear scars was found to become increasingly metallic as the contact size became larger and the oxygen was more effectively excluded. The oxygen exclusion concept outlined by Warmuth et al. [20] has since been expanded upon by Fouvry et al. [13] and Baydoun et al. [24] into a "contact oxygenation" description of wear mechanisms in fretting, incorporating the concept of "air distilling" outlined by Mary et al. [25] in which interfacial oxygen concentration becomes depleted due to reactions with exposed metal to form oxide debris. The resulting low oxygen concentration can then lead to (first-body) metal-metal contact, resulting in adhesive transfer and, therefore, to a change in wear mechanism. This interfacial oxygen concentration (IOC) concept outlined by Fouvry et al. [13] was first applied to Ti-6Al-4V contacts and has since been employed to describe similar mechanism changes in steel pairs over a wide range of conditions [15,23]. Recent work [26] has indicated that there are a number of processes that need to act in concert for wear to proceed, and that the wear rate observed in fretting is simply that rate of the slowest of those processes (this being termed the rate determining process); in that work, only the rates of debris formation and debris ejection from the contact were considered but it has since been suggested that oxygen-transport into fretting contacts should also be considered as a potential rate-determining process [27].

The effect of frequency on the nature and behaviour of debris in fretting wear is complex due to its impact both on the temperature in the contact (affecting rates of processes such as oxidation, sintering of debris particles into debris beds etc.) and on the time that contacts are exposed to wear (affecting the transport of oxygen into the contact and also the times in which processes such as oxidation and debris sintering can take place) [27]. The influence of frequency on wear rate in fretting has been observed to be impacted by other contact conditions, such as the aforementioned effect of initial contact size [20], and has been found to be greater for larger displacement amplitudes [17,28,29], although the mechanism that causes the latter effect is less clear.

Despite being fundamental in the distinction of fretting wear from other forms of sliding wear, experimental observations of the role of displacement amplitude in fretting vary considerably, but

there is general agreement that (in contrast to reciprocating sliding) the wear rate is dependent on displacement amplitude [30–34]. Increasing displacement amplitude at a given frequency has a number of effects on the development of fretting wear, including: (i) promoting debris expulsion from the contact which then affects the tendency for particles to form a layer within the contact which limits metal-metal contact between the first bodies; (ii) increasing the sliding velocity and therefore the frictional power dissipated which results in higher contact temperature (whilst reducing time between asperity interactions); (iii) increasing the proportion of the contact area that is exposed to the atmosphere with each fretting cycle (although this may still remain very small depending upon the contact configuration).

The increase in contact temperature associated with increased displacement amplitude gives rise to effects which compete in terms of wear rate. An increase in temperature tends to promote the formation of oxide wear debris which may lead to an increase in wear rate if the debris is able to readily leave the contact. However, an increase in temperature may also result in an increase both in the cohesive forces between debris particles and in the rates of sintering of that debris within the contact, which together lead to debris retention in the contact; this retained debris may form a glaze layer which generally leads to a substantial reduction in wear rate [35–42]. The formation of a stable debris bed (which limits first-body contact and therefore limits TTS formation) with a low rate of expulsion from the contact (which results in low wear) is also influenced by the slip amplitude; it has been demonstrated [36] that as displacement amplitude was increased in a fretting contact (all other controlled parameters being held constant), there was an associated *increase* in the temperature at which a stable debris bed was able to form (resulting in both low wear and limited sub-surface damage), with this being associated with changes in the relative rates of debris expulsion from the contact and debris sintering within the contact.

In another vein, it has been argued that a temperature increase in a fretting contact may also affect wear processes by causing a reduction in yield strength of the first-body materials, although it was observed by Pearson et al. [35] that for the same steel as employed in the present work (S132), only a relatively modest decrease in hardness (~14%) occurs with an increase in temperature from room temperature up to 300°C.

As outlined, there are complex and competing influences upon the physical processes controlling damage and degradation in fretting; however, work to deconvolute these can aid in the development of improved understanding of the dominant physical processes which determine damage and rates of wear and therefore provide foundations for the development of phenomenologically consistent predictive models.

In the present work, we seek to improve the understanding of the interacting effects of frequency and displacement amplitude in fretting of a high strength steel by examining changes in the nature of wear scars and ejected debris resulting from changes in these parameters.

2 Methodology

2.1 Experimental procedure

Tests were conducted on a high strength steel (BS S132), for which the composition and mechanical properties are listed in Table 1 and

Table 2 respectively. The steel was heat treated using a heat treatment cycle that has been outlined in previous work [43].

Table 1. Chemical composition of BS S132 (wt%) [43]

C	Si	Mn	P	Cr	Mo	Ni	V	Fe
0.35-0.43	0.1-0.35	0.4-0.7	<0.007	<3.0-3.5	0.8-1.1	<0.3	0.15-0.25	Balance

Table 2. Mechanical properties of BS S132 where symbols have their usual meaning in this context [44]

σ_y / MPa	σ_{ut} / MPa	HV30	E / GPa	v
1247	1697	485 ± 10	206.8	0.28

Specimen pairs were arranged in a cylinder-on-flat configuration as shown in Figure 1, with a cylinder radius, R = 6 mm and flat specimens with a width of 10 mm, generating an initial line contact with length, L = 10 mm oriented perpendicular to the fretting direction. Cylindrical and flat specimens were machined to a surface roughness (Ra) of 0.4 – 0.7 µm and 0.1 – 0.3 µm respectively. Immediately prior to tests, specimens were thoroughly degreased with detergent, and then cleaned with acetone and industrial methylated spirit (IMS) and air dried.

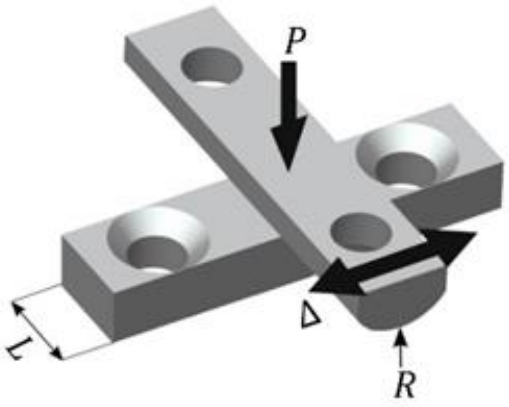

Figure 1. Cylinder-on-flat specimen configuration used in fretting tests; L = 10 mm, R = 6 mm.

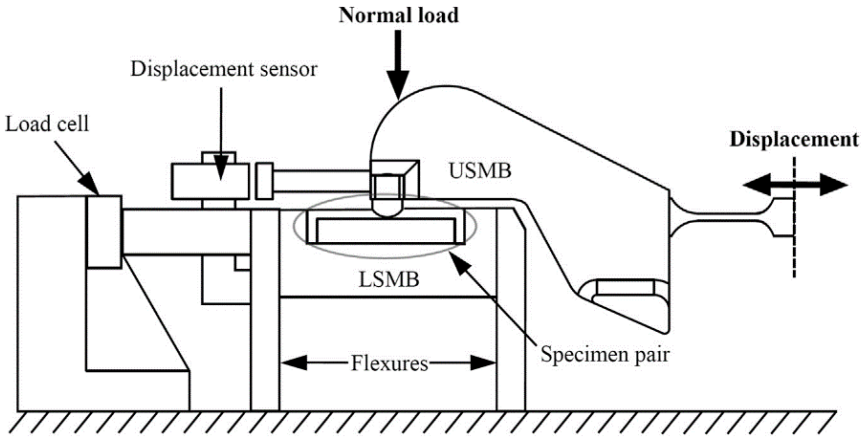

Figure 2. Schematic diagram of the main components of the fretting rig used in this study

A schematic diagram of the rig used for the tests conducted in this study is shown in Figure 2. Flat specimens were mounted onto the lower specimen mounting block (LSMB) and the cylindrical specimens onto the upper specimen mounting block (USMB), with a constant normal load (P) being applied to the USMB by a dead weight and a lever arm. Displacement was generated by an electromagnetic vibrator (EMV) at a fixed frequency, measured by a CS08 Micro-Epsilon capacitance sensor to control the relative displacement between specimens. The tangential force in the contact was measured by a Kistler 9132BA slimline piezoelectric load cell and a Kistler 5073A charge amplifier. Force and displacement data were sampled at 200 points per fretting cycle to generate fretting (i.e. hysteresis) loops and other relevant data for post-test analysis. It should be noted that in the testing system used in this study, applied displacement (Δ), as opposed to actual slip displacement at the interface (δ), is controlled during the test and therefore the latter must be derived after completion of tests to take into account compliance of the system. Moreover, to assess the impact of test parameters on friction over the total number of cycles (N) and total energy dissipated (E_d), the energy coefficient of friction (μ_E) [45] was derived using the applied normal load (P) and the slip amplitude at the interface (δ) as follows:

$$\mu_E = \frac{1}{4P\delta}\frac{dE_d}{dN} \qquad \textit{Eq. 1}$$

The test conditions employed in this study are shown in Table 3. All tests were conducted at room temperature (typically 20 °C – 25 °C). In line with our prior practice, repeat tests were conducted for selected sets of conditions to enable the variability in the wear volumes and mechanisms to be assessed; low levels of variability were observed as has been reported previously [46].

Table 3. Test conditions used in this study

Frequency, f (Hz)	20, 100, 200
Applied displacement amplitude, Δ^* (µm)	25, 50, 100
Applied normal load, P (N)	450
Test duration, N (cycles)	10^6
Temperature, T (°C)	20 - 25

Under these test conditions, the initial Hertzian contact half-width for the line contact is 54 µm. However, the scar width increases rapidly as wear occurs (due to the non-conforming nature of the cylinder-on-flat specimen geometry employed), with the relationship between the wear scar semi-width, b, and the wear volume, V_w, being well represented by the following relationship [26]:

$$V_w = L\left(R^2\, arcsin\left(\frac{b}{R}\right) - \mathrm{b}\sqrt{R^2 - b^2}\right)$$

It can be shown that even in the test which results in the smallest amount of wear (f = 200 Hz and Δ^* = 25 µm) (see Figure 4), the scar semi-width (b) has grown to more than 150 µm after only 1% of the total wear in that test has occurred and to more than 320 µm by the time that 10% of the total wear in that test has occurred.

2.2 Characterisation of damage

Upon completion of a fretting test, a sample of loose debris ejected from the contact over the course of the test was retained and stored in an airtight vial for analysis. The worn specimens were then ultrasonically cleaned in a bath of IMS to remove any debris not adhered to the worn surfaces, whereupon profilometry was then conducted using an Alicona G5 profilometer to determine the volume of material removed due to wear and assess the worn profiles of the wear scars.

Scanning electron microscopy (SEM) of the worn surface was conducted in both plan and sectional view using an FEI Quanta600 MLA SEM, using an accelerating voltage of 20 kV. Cross-sections of cylindrical specimens were obtained using an abrasive cutting wheel and prepared for metallographic examination by grinding with increasingly fine grades of silicon carbide papers, with the final finish obtained by polishing with a 1 µm diamond paste.

2.3 Ejected debris characterisation

Ejected debris retained after fretting tests was analysed using X-ray diffraction (XRD). XRD data were measured with a Siemens D500 diffractometer with Cu-Kα using a 0.04° step size between 2θ positions of 20° and 120°, with a dwell time of 22 s per step to ensure data of sufficient quality to perform Rietveld refinements to facilitate determination of the phase fractions in the debris. Rietveld refinements were performed using Topas V6 software, using the fundamental-parameters approach to X-ray line profile fitting; discrepancies in the calculated and fitted profiles attributed to complex preferred orientations in the samples were accounted for by use of a spherical harmonics function.

The size of ejected debris particles was also assessed by light diffraction using a Coulter LS230, measuring particles in the range of 375 nm to 2 mm in equivalent spherical diameter. Samples of approximately 20 mg of debris powder were dispersed in approximately 3 ml of water, then pipetted into the instrument up to a required obscuration and pumped around the 115 ml cell to obtain size measurements. Triplicate measurements were taken for each sample, and repeat tests conducted to assure the reliability of results.

3 Results

As the applied displacement amplitude (Δ^*), rather than the actual slip amplitude (δ^*) is controlled during fretting tests, it is important to clarify the extent to which changes in fretting frequency impact the actual slip amplitude to support the comparisons between conditions which will be made in this study. Figure 3(a) shows the slip amplitude for the largest nominal applied displacement of 100 µm over the range of frequencies tested, from which it is evident that fretting frequency does not have a significant impact on the slip amplitude in the employed testing configuration; moreover, the slip amplitude (δ^*) can be seen to be stable throughout the duration of tests. Figure 3(b) shows how the average slip ratio (i.e. the ratio of the slip amplitude and displacement amplitude averaged over the full duration of a test) varies over the range of conditions tested; average slip ratio is plotted against the applied displacement amplitude, with variation bars indicating the range of values across the fretting frequencies examined. In all cases, the effect of fretting frequency on slip ratio is seen to be small, and it is therefore appropriate to make comparisons between tests conducted with different displacement amplitudes and frequencies. It is noted that slip ratio is greater at larger displacement

amplitudes, which is a result of the relative impact of system compliance on slip amplitude and does not impact the validity of comparisons between displacement conditions.

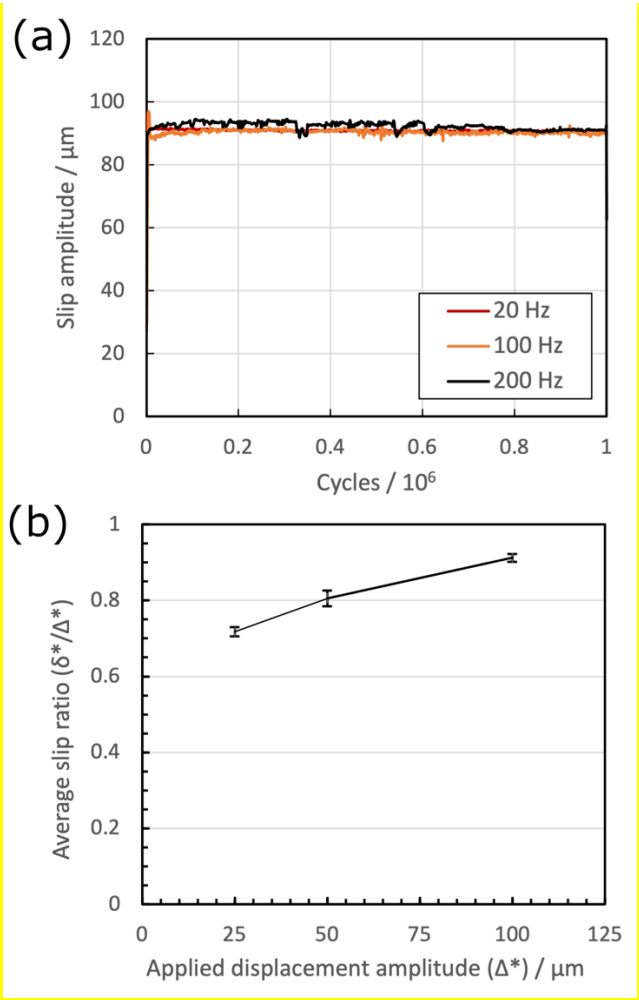

Figure 3. (a) Evolution of slip amplitude (δ^*) with number of fretting cycles with a nominal applied displacement amplitude of 100 µm over the range of fretting frequencies tested; (b) the average slip ratio as a function of displacement amplitude across the frequencies examined, with the range at each displacement amplitude indicating the variation across those frequencies.

The wear volumes following 10^6 fretting cycles across the range of frequencies and displacement amplitudes examined in this study are shown in Figure 4, presented in the commonly employed [1] form of wear volume (total net material removed from both specimens) against energy dissipated throughout the tests (with higher dissipated energies reflecting higher displacement amplitudes). The variability of the data presented in Figure 4 is in each case no more than 4% of the average value for the wear volume whilst the variation in dissipated energy is in each case no more than 10%. The confidence limits relating to these experimental measurements are in line with those determined in previous work employing the same rig used in this study, in which variation in wear in repeat tests of no more than 15% was observed [46]. Figure 4 indicates a significant difference in the evolution of wear volume with energy dissipated for the tests at 200 Hz compared to the tests conducted at 20 Hz and 100 Hz.

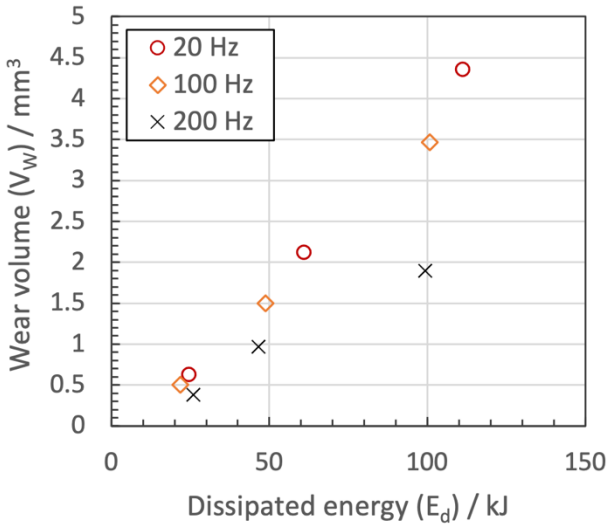

Figure 4. Wear volume after 10^6 fretting cycles as a function of dissipated energy for the three fretting frequencies examined in this study; the three values of dissipated energy for each fretting frequency relate to the three displacement amplitudes employed in the tests (namely 25 μm, 50 μm and 100 μm).

The evolution of the energy coefficient of friction throughout various tests are shown in Figure 5. At an applied displacement amplitude of 25 µm (Figure 5a), μ_E is observed to increase from ~ 0.6 to ~ 0.8 over a brief initial period (up to around 10 000 fretting cycles) and then to not change significantly over the remainder of the test; moreover, it is also seen that μ_E (and its evolution across the tests) is broadly independent of the fretting frequency. At the two higher applied displacement amplitudes (50 µm and 100 µm), μ_E is observed to be dependent upon the fretting frequency, with higher frequencies resulting in a reduction in μ_E. In comparing the traces across the three parts of Figure 5, it is notable that at 20 Hz, μ_E is not strongly dependent upon the applied displacement amplitude (~ 0.77 – 0.8 for all three applied displacement amplitudes) whereas at the two higher displacement amplitudes, μ_E is observed to decrease with increasing fretting frequency. Moreover, the values of μ_E for the two higher frequencies are both lower for the tests conducted with an applied displacement amplitude of 100 µm than for tests conducted with the smaller applied displacement amplitude of 50 µm. At the largest displacement amplitude (100 µm) and highest frequency (200 Hz), μ_E is observed to be highly unstable, exhibiting significant repeated fluctuations (> 0.1) over periods, typically of ~ 30 000 cycles, for the majority of the test. It is noted that the value of μ_E plotted every 1000 cycles indicating that the periodic variation in μ_E is a real effect and not an artifact of the data analysis.

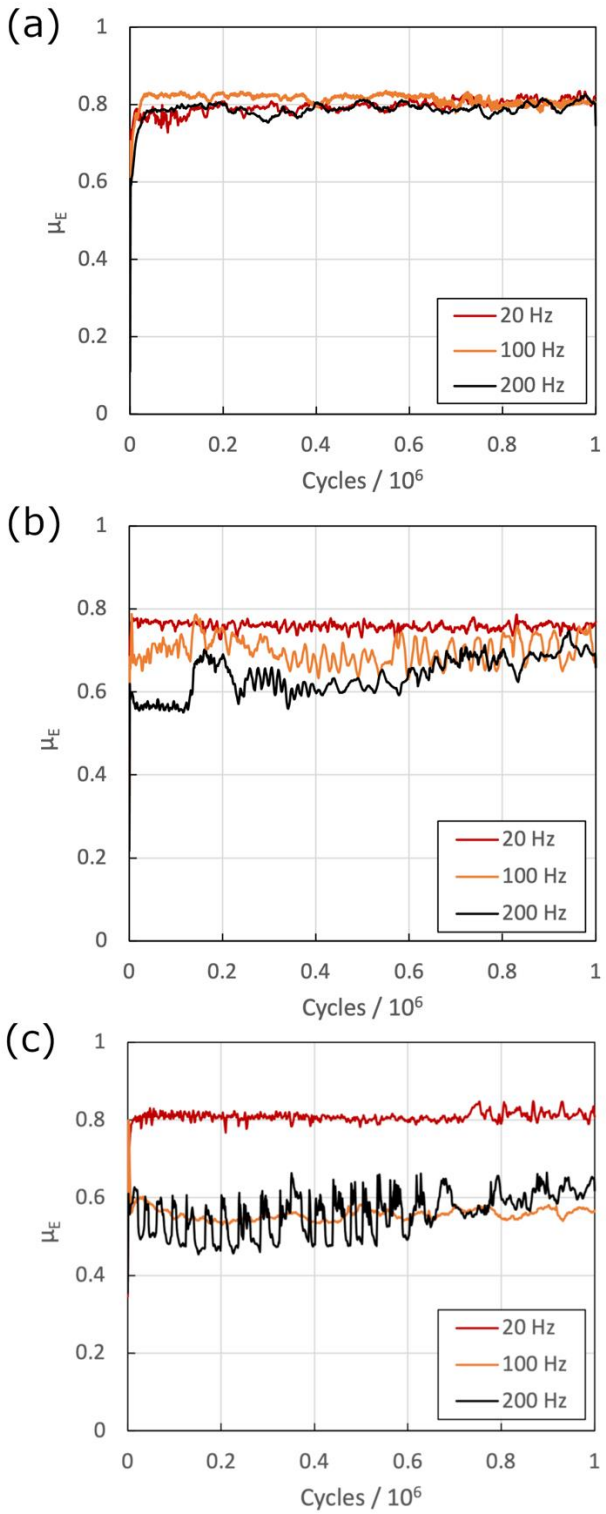

Figure 5. Evolution of energy coefficient of friction (μ_E) with number of fretting cycles at displacement amplitude (a) 25 μm; (b) 50 μm; (c) 100 μm over the range of frequencies tested in this study, showing an increasingly significant influence of both frequency and displacement amplitude on friction as both parameters are increased.

Surface profiles, presented in Figure 6, show changes in wear scar shape with fretting frequency for tests conducted with an applied displacement amplitude of 50 µm; at both extremes of the frequency range examined (20 Hz and 200 Hz), the wear scars exhibit significant variations in surface height across their length, but at the higher frequency, there is an overall reduction in wear depth, and

regions along the centre of the scar become raised relative to the maximum wear depth, which is not observed in the scars at low frequency (f = 20 Hz).

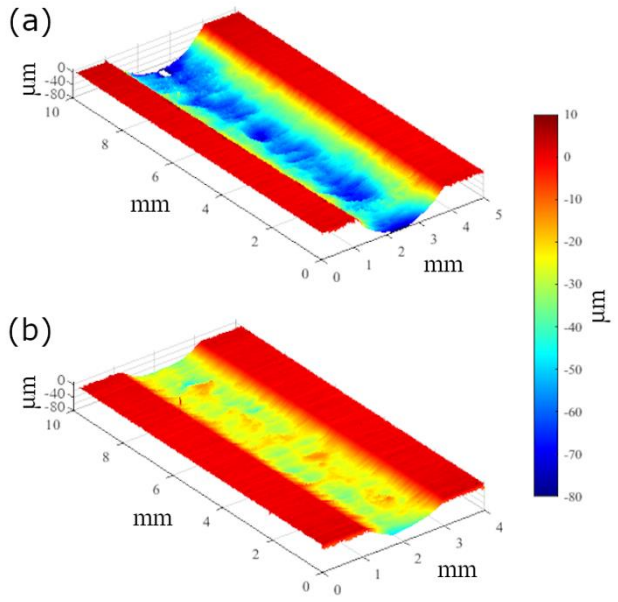

Figure 6. 3D surface profiles of wear scars on the flat specimens after fretting for 10^6 cycles with an applied displacement amplitude of 50 μm with frequencies of (a) 20 Hz; (b) 200 Hz.

Wear scar shapes can be reasonably represented by average profiles calculated from the 3D profiles of the type shown in Figure 6, with these being shown for all test conditions in Figure 7. These average profiles show scars becoming increasingly W-shaped at low displacement amplitude as frequency is increased, with the effect becoming less pronounced at the higher displacement amplitudes; it is noted that at the highest displacement amplitude examined (Δ^* = 100 μm), the scar remains U-shaped across the range of fretting frequencies examined.

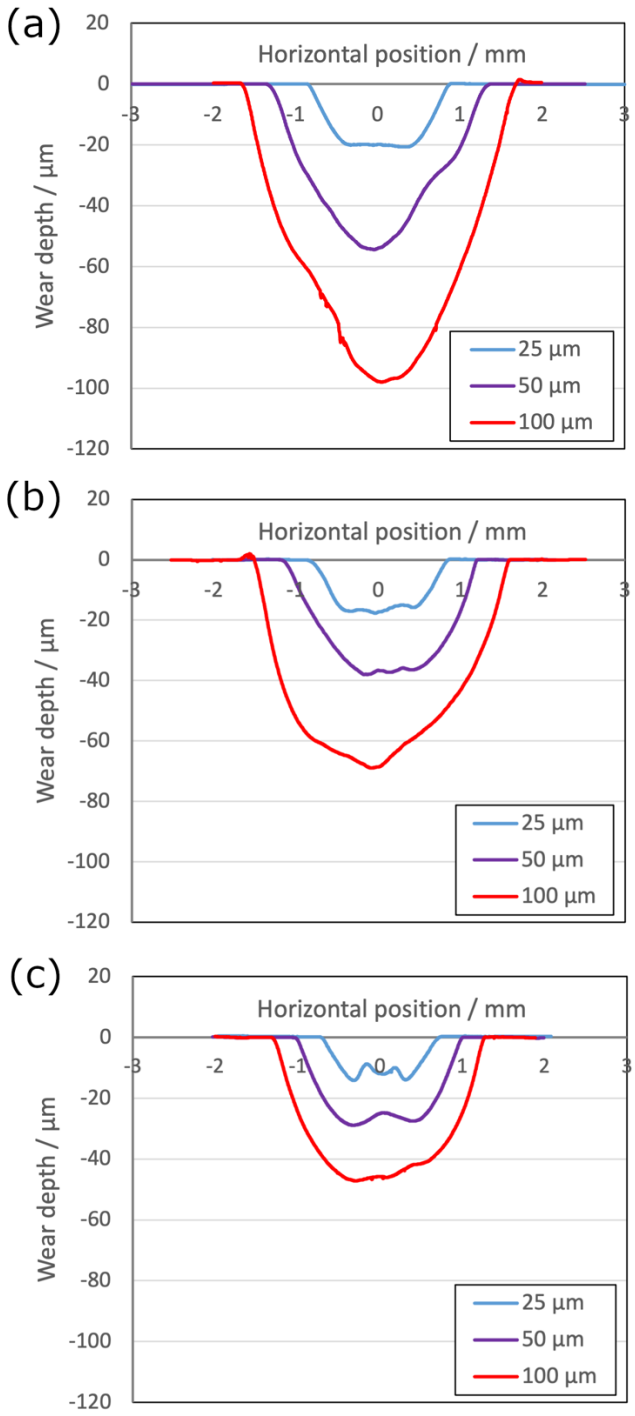

Figure 7. Average wear scar profiles of flat specimens after fretting for 10^6 cycles with three different applied displacement amplitudes and with frequencies of (a) 20 Hz; (b) 100 Hz; and (c) 200 Hz. A transition from U-shaped scars to more W-shaped wear scars is observed with decreasing displacement amplitude and increasing frequency.

The change in scar shape from U-shaped to W-shaped has been reported by others in the literature [13,15,23], and has been attributed to a transition from (i) an abrasive wear mechanism (in which sufficient oxygen is present at the interface to continually form oxide, which acts as an abrasive and is subsequently ejected from the contact) resulting in U-shaped scars, to (ii) an adhesive mechanism (in which there is insufficient oxygen at the interface to generate a layer of oxide debris to separate

surfaces, leading to metal-to-metal contact and transfer of metal between surfaces) resulting in W-shaped scars.

Plan view BSE SEM micrographs of the wear scars on the flat specimens are presented in Figure 8. It can be seen from these images that when displacement amplitude is small (Δ^* = 25 μm), wear scars are covered by a coherent bed of oxide debris, identifiable as such by its darker grey colour, (associated with the lower average atomic number associated with oxides when compared to metals) across the range of frequencies tested in this study. Similarly, at low frequency (f = 20 Hz), scars are also covered by debris beds consisting primarily of oxide. Some bright (i.e. metallic) regions can be seen interspersed with the oxide debris in the scars formed under these conditions (particularly at low frequency) with these indicating areas where beds have broken down; however, despite these, oxide coverage is fairly uniform, with oxide covering the central regions of the scar as well as the edges. It should be noted that after fretting tests, the specimens were ultrasonically cleaned to remove non-adhered debris, and therefore it is not clear whether such areas were actually exposed during the fretting tests themselves.

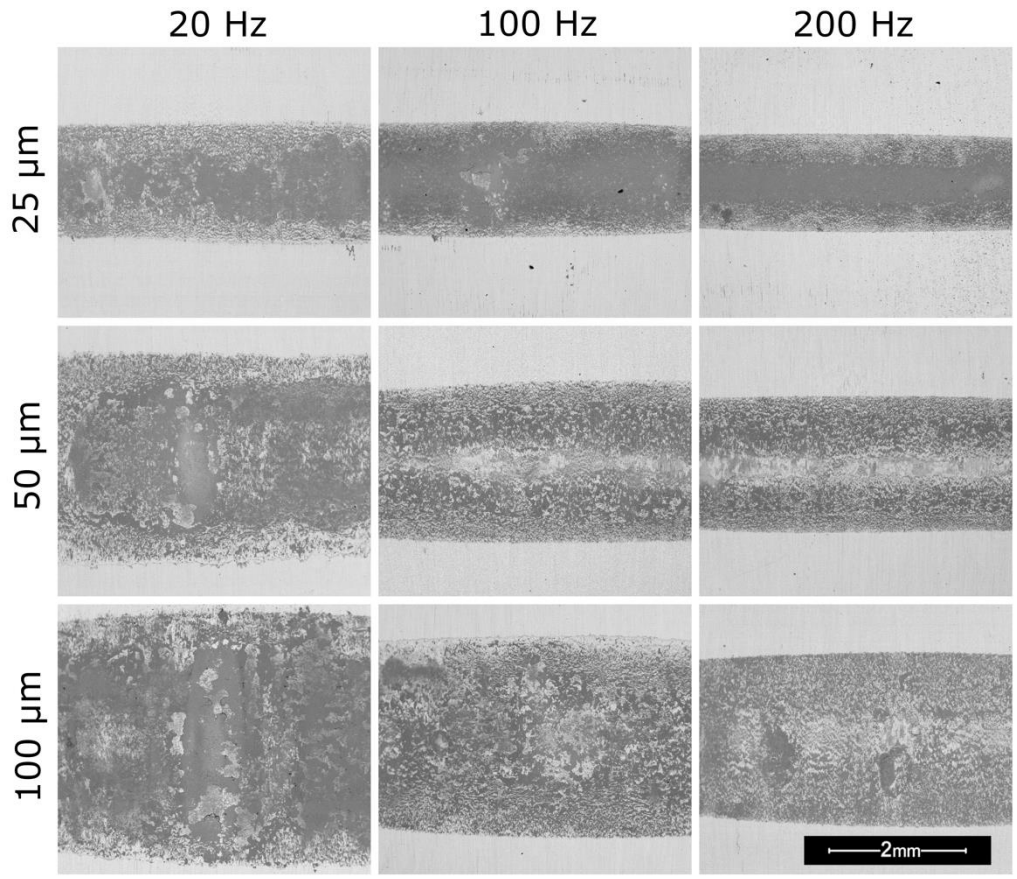

Figure 8. Plan view BSE SEM micrographs of wear scars on flat specimens after fretting for 10^6 cycles over the range of frequencies and displacement amplitudes examined in this study, showing a marked difference in the nature of the debris beds, with a tendency towards reduced oxide coverage at larger displacement amplitudes and higher frequencies, and an associated increase in exposed metallic surfaces.

At low displacement amplitude (Δ^* = 25 μm), as frequency is increased the oxide-dominated debris beds appear to become more coherent and can be seen to correspond to more W-shaped scars (Figure

7), indicating that under these conditions, the raised central region consists at least partially of retained oxide debris.

As both the frequency and displacement amplitude are increased, it can be seen that debris beds become less uniform and that the scars become increasingly metallic, particularly in the central regions where oxygen access is most restricted. At the intermediate displacement amplitude (Δ^* = 50 μm), the central regions of the scars developed at the two higher frequencies are largely metallic, and are particularly distinct from the darker oxide-based regions nearer the edges; as with the oxide-based scars formed at low displacement amplitude, these features correspond to raised regions observed in the averaged profiles in Figure 7, which suggests that the raised regions consist at least partially of transferred metal. As displacement amplitude is further increased to 100 μm, this difference in composition between the central region and the rest of the scar is less defined, and profiles become U-shaped, indicating an abrasive wear mechanism.

The impact of displacement amplitude on the nature of surfaces formed at the highest frequency of 200 Hz is presented in greater detail in Figure 9, which shows central regions of wear scars at higher magnification. At low displacement amplitude (Δ^* = 25 μm), when an oxide debris bed covers the surface, no cracking is visible at the surface; however, at the two higher displacement amplitudes, where oxide coverage is limited, the exposed metallic surfaces are severely cracked.

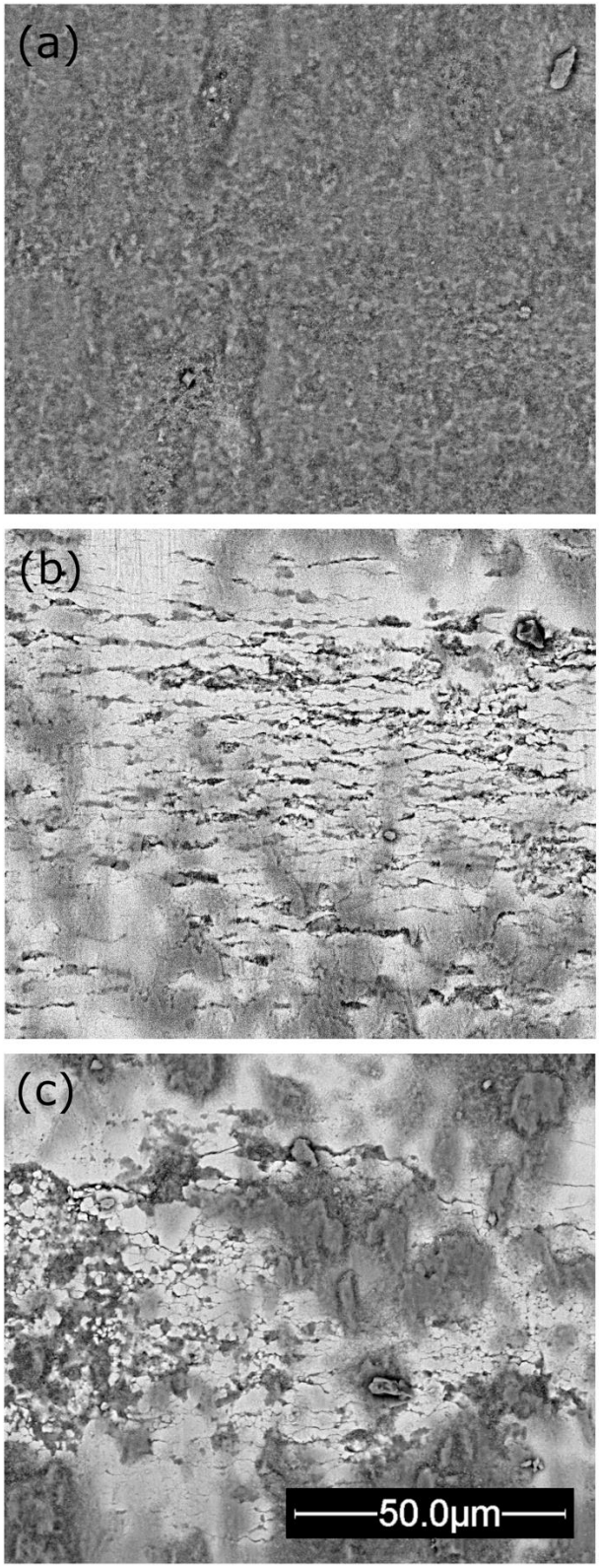

Figure 9. High magnification BSE SEM micrographs of wear scars on flat specimens in plan view after fretting at high frequency (f = 200 Hz) for 10^6 cycles with an applied displacement amplitude of: (a) 25 µm; (b) 50 µm; (c) 100 µm.

Cross-sections through wear scars on the cylindrical specimens are presented in Figure 10 in the same format as the plan view images in Figure 8. The scars formed by fretting with a displacement amplitude of 25 µm (for all three fretting frequencies) and by fretting at a frequency of 20 Hz (for all three applied

displacement amplitudes) consist of an oxide debris bed adhered to the largely undeformed metallic specimen. However, for the remaining samples (higher frequencies and higher displacement amplitudes), a thick layer of severely damaged metallic material is also observed which is termed the tribologically transformed structure (TTS) [13,16]. Comparison with cross-sections of flat specimens indicate that the severely damaged layer of metallic material occurs in both the flat and cylindrical specimens of the pair.

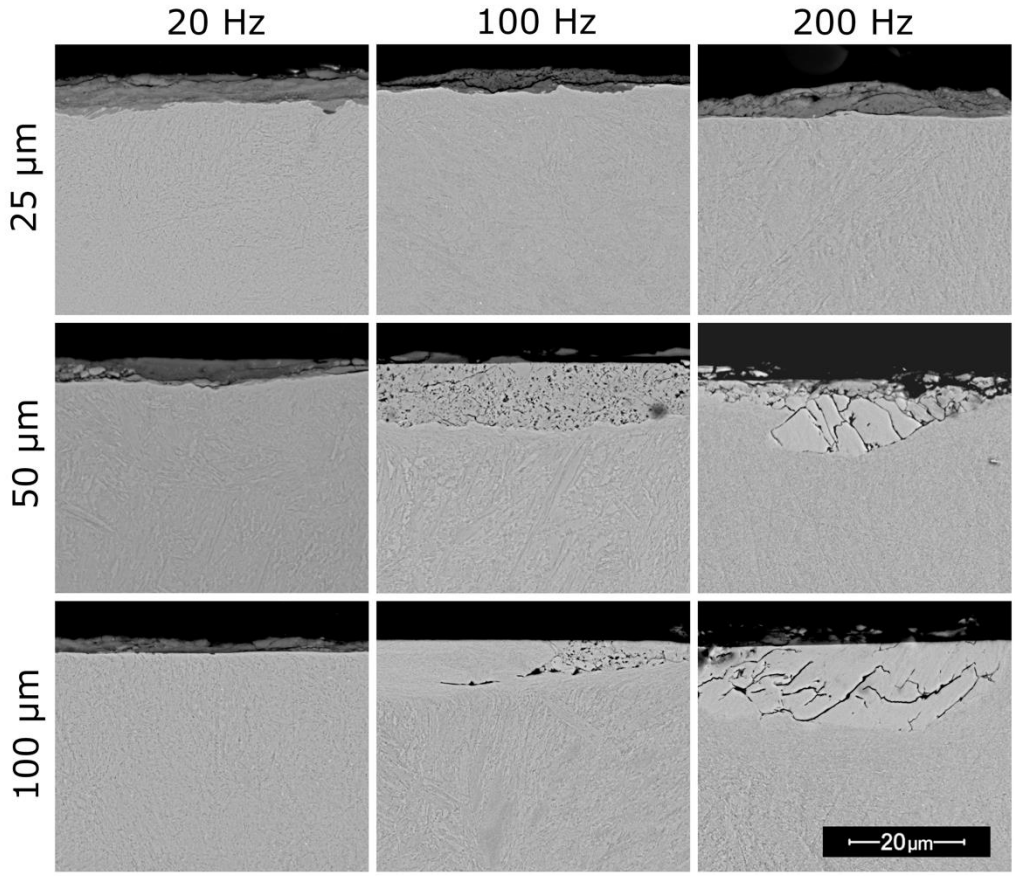

Figure 10. BSE SEM micrographs in sectional view of wear scars in cylindrical specimens after fretting for 10^6 cycles over the range of frequencies and applied displacement amplitudes examined in this study, showing the development of significant levels of subsurface damage associated with increases in both parameters.

The subsurface damage after fretting under the most extreme conditions tested (f = 200 Hz; Δ^* = 100 µm) is presented in greater detail in Figure 11, which shows extensive cracking in a transformed metallic region extending approximately 20 µm below the surface. In this region, there is little evidence of any of the original martensitic lath structure remaining in the metal, indicating that the original microstructure has been heavily modified. There is a sharp boundary between the damaged metal and the bulk metal, both in terms of the differences in the basic microstructure (martensitic versus featureless) and in terms of the damage (uncracked versus cracked). This sharp boundary suggests that the layer has been formed at least in part by adhesive transfer, but due to the like-on-like nature of the specimen pairs employed in this study, this cannot be conclusively determined from the evidence available. There is an oxide debris bed atop the damaged metal, but it appears to be highly fragmented in contrast to the coherent layers observed under low displacement and low frequency fretting conditions (Figure 10).

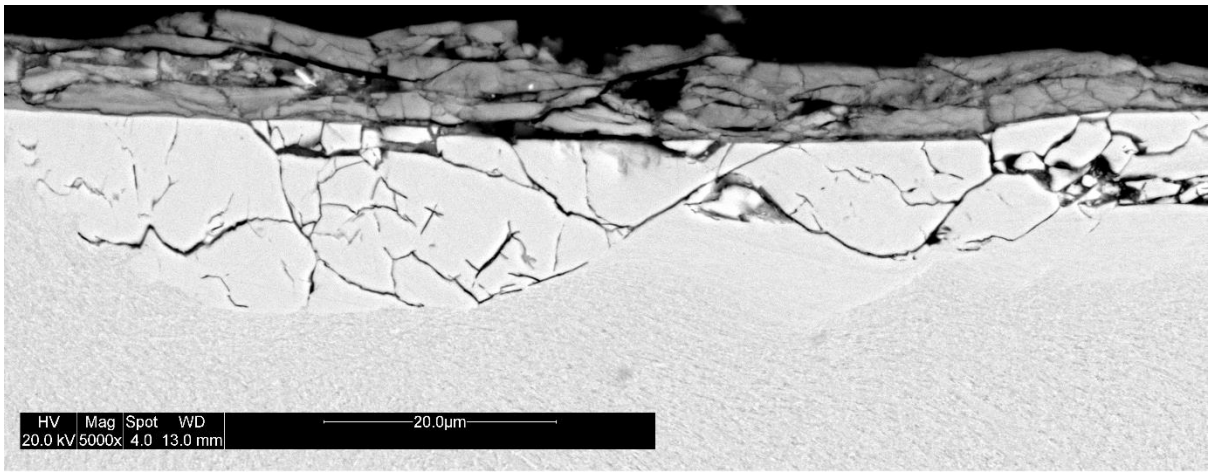

Figure 11. BSE SEM micrograph in sectional view of the wear scar in a cylindrical specimen fretted at high frequency (f = 200 Hz) and high displacement amplitude (Δ^* = 100 µm), showing extensive cracking in the near surface region in which there is little evidence of the original martensitic microstructure.

Analysis of ejected debris by X-ray diffraction showed that under all conditions tested, only two phases were present in the debris, namely iron oxide, α-Fe_2O_3, and metallic iron, α-Fe. Figure 12 shows the weight fraction of metallic iron in the samples of ejected debris, as calculated by Rietveld analysis, and shows that at all displacements tested, a modest reduction in the metallic content of ejected debris can be seen with increasing fretting frequency. Also, the metallic content is observed to increase with increasing displacement amplitude across the range of frequencies examined.

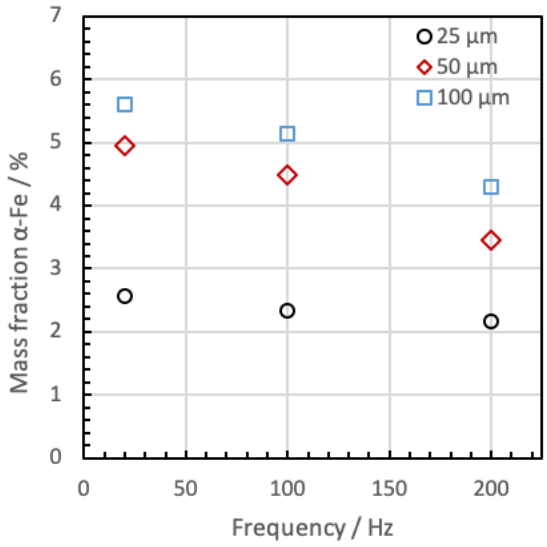

Figure 12. Plot of estimated ferrite mass fraction in the loose debris collected following fretting for 10^6 cycles for all combinations of displacement amplitude and fretting frequency examined in this study, showing a decrease in the metallic content of ejected debris as frequency is increased and as the fretting displacement amplitude is reduced.

Figure 13 shows the mean diameter of particles in the ejected debris samples, as calculated from measured particle size distribution data; at all displacement amplitudes examined, average particle size decreased with increasing frequency. Moreover, the average particle size appears not to depend strongly on displacement amplitude, with no significant difference in particle size between

displacement amplitudes of 50 μm and 100 μm, and only a relatively small reduction in particle size as displacement amplitude is reduced from 50 μm to 25 μm.

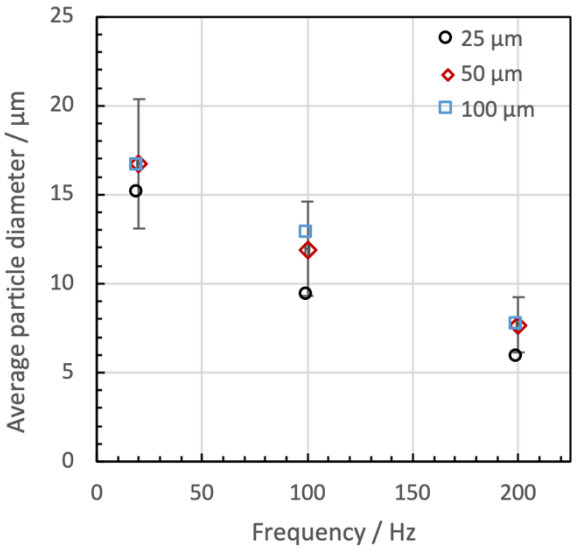

Figure 13. Plot of mean diameter of loose debris particles collected following fretting for 10^6 cycles for all combinations of displacement amplitude and fretting frequency examined in this study, showing a decrease in particle size as frequency is increased for all displacement amplitudes tested.

4 Discussion

4.1 Summary of observed behaviour

Two broad classes of behaviour have been observed in the tests conducted, related to the nature of the wear scar surface, the nature of the sub-surface damage below the wear scar and the energy coefficient of friction, μ_E. Clear correlation exists between these three features and a summary of these observations for the various test conditions is presented in Table 4. Two broad regimes are identified.

- In Regime I (indicated by light grey shading in Table 4), the scar surface is dominated by oxide, there is limited sub-surface damage and a high value of μ_E is observed;
- In Regime II (indicated by the unshaded cells in Table 4), the scar surface has a much higher area fraction of metal, there is extensive sub-surface damage and a reduced value of μ_E is observed.

Table 4 Summary of the features observed in fretting under the various test conditions examined. Two broad regimes are identified, with shading indicating whether observed behaviour aligns with Regime I (light grey) or Regime II (unshaded).

		Fretting frequency		
		20 Hz	100 Hz	200 Hz
Applied displacement amplitude	25 µm	• Oxide scar surface • Limited sub-surface damage • High value of μ_E	• Oxide scar surface • Limited sub-surface damage • High value of μ_E	• Oxide scar surface • Limited sub-surface damage • High value of μ_E
	50 µm	• Oxide scar surface • Limited sub-surface damage • High value of μ_E	• Metallic scar surface • Extensive sub-surface damage • Reduced value of μ_E	• Metallic scar surface • Extensive sub-surface damage • Reduced value of μ_E
	100 µm	• Oxide scar surface • Limited sub-surface damage • High value of μ_E	• Metallic scar surface • Extensive sub-surface damage • Reduced value of μ_E	• Metallic scar surface • Extensive sub-surface damage • Reduced value of μ_E

The extensive sub-surface damage is only observed in cases where the wear scar surface is predominantly metallic (i.e. where an oxide debris bed to separate the first bodies fails to develop). It is proposed that the failure to develop the debris bed results in the development of extensive sub-surface damage. Moreover, the coefficient of friction is associated with the nature of the surfaces; the development of an oxide bed which separates the first bodies results in a higher coefficient of friction whereas the failure to develop such an oxide bed (resulting in a predominantly metallic contact) results in a lower coefficient of friction.

As outlined previously, it is clear that the behaviour observed (with its root-cause dependence upon the formation of an oxide-based debris bed in the contact which separates the first bodies and limits their resulting sub-surface deformation) depends both upon the fretting frequency and upon the displacement amplitude. This discussion will attempt to describe the influence of these test parameters upon the tendency to form such an oxide debris bed.

4.2 Role of frictional power dissipation

It is noted that Regime II relates to both high applied displacement amplitudes and high fretting frequencies, which both affect frictional power dissipation in the contact. It must therefore be considered whether it is in fact high frictional power dissipation in the contact (generated by that combination of high displacement amplitude and high frequency) which actually results in Regime II behaviour.

An examination of the test matrix indicates that (assuming that the coefficient of friction is similar) the power dissipated under conditions where Δ^* = 25 µm and f = 200 Hz (in Regime I) is broadly the same as that dissipated under conditions where Δ^* = 50 µm and f = 100 Hz (in Regime II). The fact that the behaviour observed is in Regime I in one case and Regime II in the other indicates that it is not the frictional power dissipation itself which determines the regime.

To examine this further, an additional test was conducted under conditions of Δ^* = 50 µm and f = 100 Hz but where the frictional power dissipation was reduced not by changing either of these variables,

but by reducing the applied load from the standard value of 450 N to 250 N. Again, assuming that the coefficient of friction does not change significantly, the power dissipated under conditions where Δ^* = 50 µm, f = 100 Hz and P = 250 N is similar to that where Δ^* = 25 µm, f = 100 Hz and P = 450 N. This comparison has the advantage of being able to explore the role of power dissipation without changing other key factors affected by frequency and displacement, such as the time between asperity interactions.

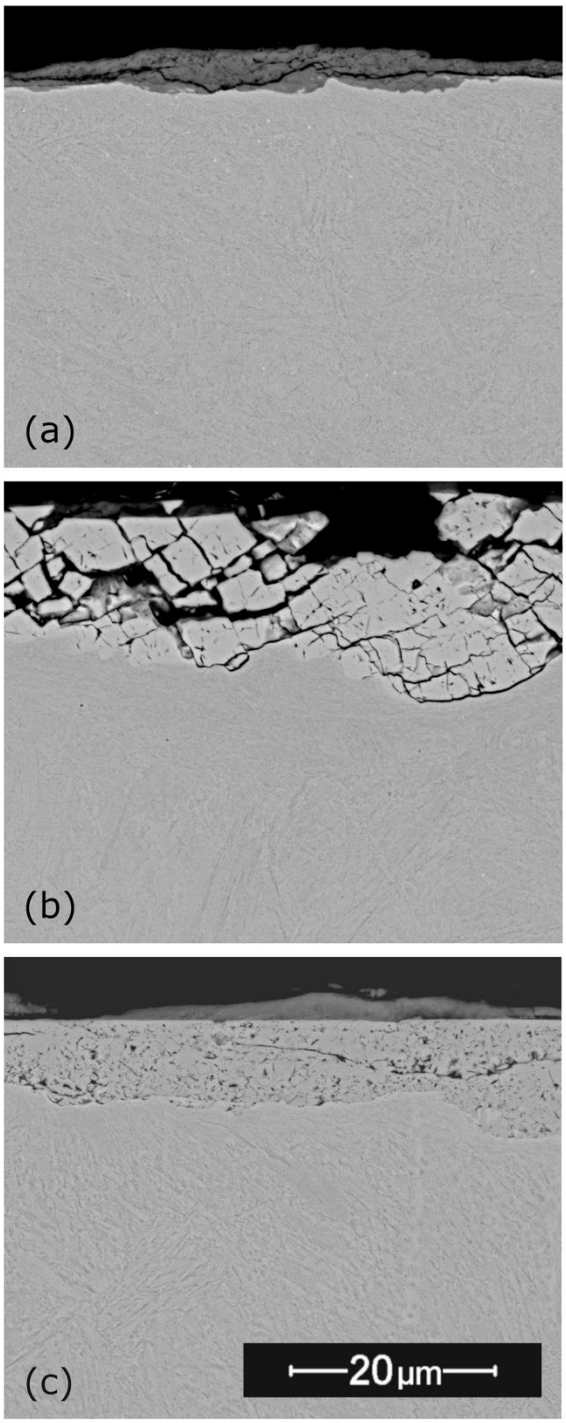

Figure 14. BSE SEM images in sectional view of wear scars in cylindrical specimens after fretting under different combinations of displacement amplitude and normal load: (a) Δ^* = 25 µm, P = 450 N; (b) Δ^* = 50 µm, P = 250 N; (c) Δ^* = 50 µm, P = 450 N; showing significant variation in the extent of subsurface damage that develops (f = 100 Hz; N = 10^6 cycles).

Table 5 Comparisons which can be made within Figure 14

Comparisons available in Figure 13	Applied displacement amplitude	Fretting frequency	Frictional power dissipation	Damage regime
(a) and (b)	Different	Same	Similar	Different
(b) and (c)	Same	Same	Different	Same

Cross-sections of the specimens worn under three sets of conditions are presented in Figure 14, with Table 5 suggesting appropriate comparisons which can be made between the test conditions and sub-surface damage observed in the tests presented in Figure 14. A comparison of Figure 14 (a) and (b) where the frictional power dissipation is similar reveals very different sub-surface damage (associated with the difference in applied displacement amplitude); moreover, comparison of Figure 14 (b) and (c) where the frictional power dissipation is different reveals very similar sub-surface damage (associated with the fact that the applied displacement amplitude is the same in both cases). As such, it is argued that the transitions between Regime I and Regime II are associated with changes in fretting frequency and with changes in displacement amplitude, and not causally with changes in frictional power dissipation.

4.3 The combined role of frequency and displacement amplitude on development of an oxide-based debris bed to limit direct first-body interaction

Previous work on the role of frequency in fretting wear, using the same material and specimen configuration used in this study, has noted that increased frequency results in debris retained in wear scars becoming increasingly metallic [20] and (after an extended number of cycles) to result in significant changes in the development of subsurface damage [14]. In the present work, it is seen that the effect of frequency on the development of debris beds and subsurface damage in fretting wear is also significantly impacted by displacement amplitude.

A significant reduction in wear volume at a given dissipated energy was observed with increasing frequency (Figure 4). The reduction in wear with frequency is not steady, with a much greater reduction as frequency is increased from 100 Hz to 200 Hz than between 20 Hz and 100 Hz. These changes in wear do not correlate strongly with changes in damage mechanism (Figure 10) or the composition of ejected debris (Figure 12), which although affected by both frequency and displacement amplitude, consists mostly of oxide (>94%) under all conditions tested, indicating that no transition to a severe wear regime takes place in which large metallic debris particles are ejected.

The impact of frequency on debris bed coverage (and in turn wear scar shape) is markedly different at high and low displacement amplitudes; at low displacement amplitude (Δ^* = 25 μm), wear scars are oxide-dominated and can be seen to become more coherent (i.e. exhibiting fewer exposed metallic regions) as frequency is increased (Figure 8 and Figure 9) corresponding to increasingly W-shaped wear scars (Figure 7). This contrasts with the behaviour observed at high displacement amplitude (Δ^* = 100 μm), in which increasing frequency results in debris beds becoming sparser, while remaining U-shaped.

A change in wear mechanism with increasing frequency, from an oxidation-dominated abrasive mechanism (resulting in U-shaped wear scars) to one in which inhibited oxygenation at the centre of the contact results in adhesive metal transfers (resulting in W-shaped scars) has been observed

previously in different materials and specimen configurations [13,14,23]. Such a transition in mechanism is observed in the present work at an intermediate displacement amplitude (Δ^* = 50 μm) but is seen to be only one of several potential effects of frequency on wear mechanism.

Both frequency and displacement amplitude have been shown in other works to significantly affect debris retention. In an experimental investigation of steel pairs with a significant difference in hardness, Lemm et al. [47] observed that a reduction in frequency from 50 Hz to 5 Hz (all other factors being equal) resulted in a change in wear mechanism from (i) one in which debris embedded in the softer surface, which subsequently wore significantly less than the harder surface, to (ii) one in which both bodies developed deep wear scars, indicative of the oxide debris being removed from the contact. This was attributed to the effect of frequency on local temperature, and the associated impact either on surface hardness (and hence ability of debris particles to embed), the rate of debris sintering to form a bed which both reduces the rate of debris expulsion from the contact and which limits direct first-body contact, or a combination of the two. Increasing displacement amplitude appears to have the opposite effect, with higher displacement amplitudes being associated with a greater rate of debris ejection; Hayes and Shipway [36] observed that increasing displacement amplitude reduces the tendency for oxide debris to sinter to form a protective bed (reduced wear and limited sub-surface damage), with this effect attributed to an enhanced rate of debris ejection.

It is proposed that the interacting effects of frequency and displacement amplitude arise not only from the impact of both parameters on the rate of debris expulsion, but rather on three key processes (of which debris expulsion is one) that determine the dominant wear mechanism: (i) ingress of oxygen to the contact; (ii) formation of oxide debris; (iii) expulsion of oxide debris from the contact. Which of these rates is lowest (and hence controls wear mechanism) will vary depending on both displacement amplitude and frequency; for example, in the case of low displacement amplitude (Δ^* = 25 μm) and low frequency (f = 20 Hz), the rate of oxygen ingress to the contact is sufficient to generate oxide debris (the low sliding velocity increases the time between asperity interactions and reduces the rate at which oxygen is consumed in the formation of oxide debris), while the relatively small increase in local temperature (associated with the low frictional power dissipation) results in the oxide being readily ejected; together, this results in an oxide-dominated, U-shaped wear scar. As frequency is increased, the ratio of the rates of oxygen ingress and wear debris formation falls; however, the local temperature increases, which promotes sintering of debris particles to form a protective debris bed (with low rates of wear and limited sub-surface damage). In this case, the rate of debris expulsion from the contact is sufficiently low that there is sufficient oxygen present to form oxide throughout the contact, resulting in an oxide-dominated, W-shaped wear scar.

In the case of larger displacements, the balance is different; at large displacement amplitude (Δ^* = 100 μm) and high frequency (f = 200 Hz), a metallic, U-shaped scar (Figure 7c) develops, indicating that the enhanced rate of debris ejection is dominant over any increase in the rate of debris sintering resulting from the increased local temperature associated with higher frictional power dissipation. Rather than a localised metallic region at the centre of the scar, an oxide bed can be seen to partially cover the whole surface (Figure 8); however, much of the underlying metallic surface remains exposed, and the significant subsurface damage observed at these conditions (Figure 10) indicates that while temperature and oxygen access are sufficient to facilitate oxide formation throughout the contact, the rate of oxide formation and of its expulsion from the contact together mean that conditions are not conducive to the formation of a debris bed which effectively separates the first-bodies from direct contact with each other.

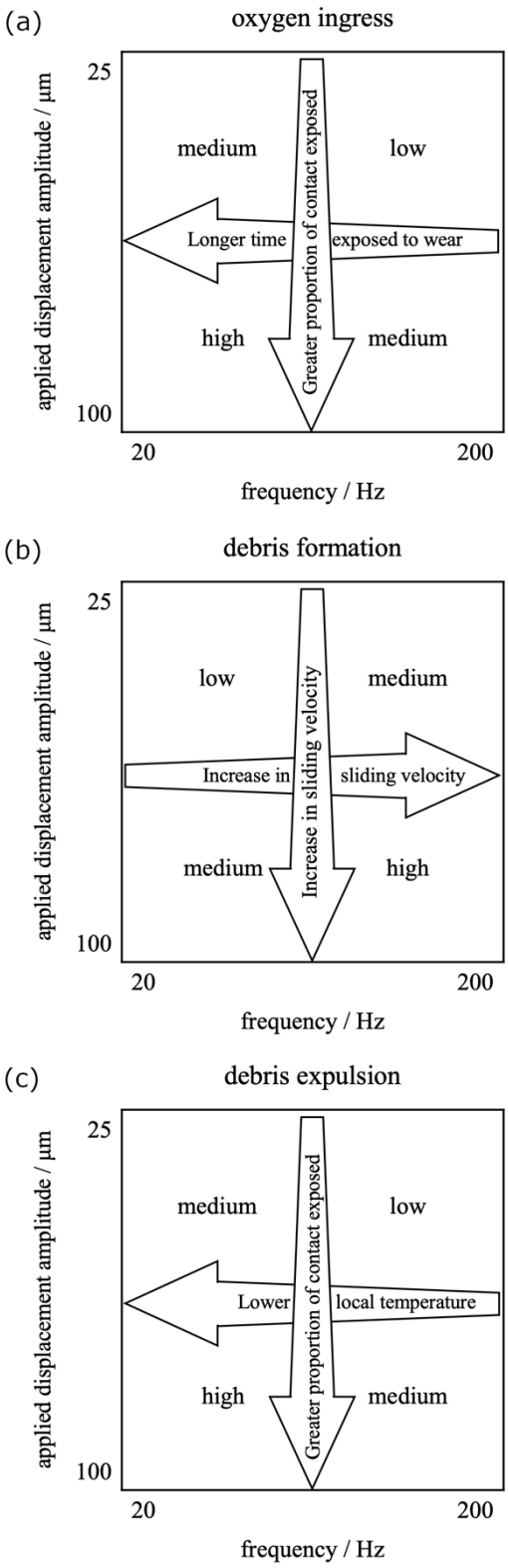

Figure 15. Phenomenological fretting map illustrating how changes in displacement amplitude and frequency affect rate-determining processes (a) oxygen ingress; (b) debris formation; (c) debris expulsion; arrows superimposed on the maps indicate changes in important physical processes affecting debris bed formation over these conditions.

To clarify the interacting effects of frequency and displacement amplitude on rate-determining processes, a series of phenomenological fretting maps is presented in Figure 15 with arrows

representing changes in key physical processes superimposed over the relative rates over the range of conditions tested in this study.

4.4 Impact on ejected debris

The changes in composition of retained debris due to changes frequency and displacement amplitude are not reflected in debris actually ejected from the contact (Figure 12). While displacement amplitude has a fairly significant effect on the proportion of ejected debris consisting of metallic iron (which, despite always being a small proportion, increases by over a factor of 2 as the displacement amplitude is increased from 25 μm to 100 μm), these changes are similar regardless of whether or not a coherent debris bed forms. This also applies to the modest reduction in metallic content as frequency is increased, in contrast to the tendency towards more metallic wear scars under the same conditions. This may be attributed to high cohesive forces between metallic particles, promoting their retention near the centre of the contact, while particles that are eventually ejected must travel to the edges where there is greater availability of oxygen, and oxidation occurs at an accelerated rate due to increased local temperature. The composition of ejected debris is therefore not fully representative of all debris formed during fretting, but serves to highlight the localised nature of changes in debris formation in areas where oxygen access is restricted.

Under all conditions tested in this study, average particle diameter of the ejected debris lies in the range of approximately 6 μm – 17 μm (Figure 13), indicating that a significant proportion of ejected debris "particles" are in fact agglomerates of many smaller debris particles, as opposed to individual pieces of wear debris. This is consistent with previous observations by the authors of ejected debris generated during fretting tests using the same material and testing system as used in this study, in which a significant degree of agglomeration and sintering of submicron oxide particles was observed [48].

The limited effect of displacement amplitude on particle size reinforces the observation based on compositional analysis of the debris that despite the change in damage mechanism under high frequency and high displacement amplitude conditions, these conditions do not result in a transition to a severe wear regime in which larger, more metallic debris particles are ejected.

4.5 Implications for future work

The present work highlights a significant degree of interaction between the effects of frequency and displacement amplitude on fretting wear, which are thought to arise due to competing effects of key rate-determining processes, namely (i) ingress of oxygen to the contact; (ii) formation of oxide debris, and (iii) expulsion of oxide debris from the contact. If wear rate may be assumed to be controlled by the relationship between these three processes, a model is required that is capable of predicting the development of fretting wear over a range of sliding conditions and contact geometries; the potential for such a model should therefore be considered in future work.

Using the same test configuration employed in this study, Zhu et al. [26] demonstrated the predictive capability of a model in which wear rate in fretting is controlled by either the rate of debris formation or its expulsion from the contact, which captured wear rate well over a range of test durations and differing contact geometries. However, the present work highlights the critical role of oxygen ingress throughout the contact in controlling the development of wear (particularly at high fretting frequencies and displacement amplitudes), which must therefore be considered in future work in this

area to develop models capable of accurately predicting wear rate over a wider range of test conditions.

Whilst the work here has only examined the fretting behaviour at ambient temperatures, it is well known that fretting at elevated temperatures results in the formation of a glaze layer by sintering of debris within the contact, and that the observed wear rate falls significantly when this takes place. This observation is in accord with the general proposal here, with the debris sintering resulting in the rate of debris expulsion from the contact falling and this being then the rate determining process.

5 Conclusions

The effect of frequency on the formation of debris beds and the development of subsurface damage in fretting wear of a high strength steel at room temperature is shown to be highly dependent on the displacement amplitude. For larger displacement amplitudes, increases in frequency result in a transition from an oxidation-dominated wear mechanism to one in which oxide debris beds which effectively limit direct contact between the first-bodies cannot form, resulting in the development of severe subsurface damage. When displacement amplitude is reduced, the same increase in frequency does not result in significant subsurface damage, with wear scars remaining oxide-dominated across the range of frequencies examined. This is attributed primarily to increased residence time of wear debris at smaller displacement amplitudes, combined with increased local temperature at higher frequencies promoting agglomeration and sintering of oxide debris to form oxide debris beds which effectively limit direct first-body interactions, in turn preventing the development of severe damage and cracking in the bulk metal.

Increasing frequency is observed to result in ejected debris particles becoming smaller in size and to contain a reduced proportion of metallic iron, with these trends being largely unaffected by displacement amplitude. This is in contrast to debris retained within contacts, which becomes more metallic at higher frequencies and displacement amplitudes; the difference between retained and ejected debris indicates that the metallic debris formed under high frequency and displacement conditions is largely retained within contacts.

The findings indicate that there is significant interaction between the impacts of frequency and displacement amplitude on fretting wear as a result of interacting effects on debris formation and ejection, and that such interactions should be considered if the physical processes or wear are to be understood and accurate predictive models developed. It is noted that the results of this study focus solely on fretting at room temperature, and further experimental investigation is required to directly validate the hypotheses made regarding the role of glaze formation in determining the rate determining process at elevated temperature.

6 Acknowledgements

The authors would like to acknowledge Rolls-Royce plc for their support and funding of this research through the Transmissions University Technology Centre (UTC) at the University of Nottingham, UK.

The authors thank the Nanoscale and Microscale Research Centre (nmRC) at the University of Nottingham for providing access to instrumentation.

7 References

[1] S. Fouvry, C. Paulin, T. Liskiewicz, Application of an energy wear approach to quantify fretting contact durability: Introduction of a wear energy capacity concept, Tribol. Int. 40 (2007) 1428–1440. https://doi.org/https://doi.org/10.1016/j.triboint.2007.02.011.

[2] M. Godet, The third-body approach: A mechanical view of wear, Wear. 100 (1984) 437–452. https://doi.org/10.1016/0043-1648(84)90025-5.

[3] M. Godet, Third-bodies in tribology, Wear. 136 (1990) 29–45. https://doi.org/10.1016/0043-1648(90)90070-Q.

[4] C. Colombié, Y. Berthier, A. Floquet, M. Godet, Fretting: Load carrying capacity of wear debris, J. Tribol. 106 (1984) 192–200. https://doi.org/10.1115/1.3260881.

[5] Y. Berthier, L. Vincent, M. Godet, Velocity accommodation in fretting, Wear. 125 (1988) 25–38. https://doi.org/10.1016/0043-1648(88)90191-3.

[6] Y. Berthier, L. Vincent, M. Godet, Velocity accommodation sites and modes in tribology, Eur. J. Mech. A/Solids. 11 (1992) 35–47.

[7] M. Varenberg, G. Halperin, I. Etsion, Different aspects of the role of wear debris in fretting wear, Wear. 252 (2002) 902–910. https://doi.org/10.1016/S0043-1648(02)00044-3.

[8] A. Iwabuchi, K. Hori, H. Kubosawa, The effect of oxide particles supplied at the interface before sliding on the severe-mild wear transition, Wear. 128 (1988) 123–137. https://doi.org/10.1016/0043-1648(88)90179-2.

[9] H. Kato, K. Komai, Tribofilm formation and mild wear by tribo-sintering of nanometer-sized oxide particles on rubbing steel surfaces, Wear. 262 (2007) 36–41. https://doi.org/10.1016/j.wear.2006.03.046.

[10] H.C. Meng, K.C. Ludema, Wear models and predictive equations: their form and content, Wear. 181–183 (1995) 443–457. https://doi.org/10.1016/0043-1648(95)90158-2.

[11] V. Nurmi, J. Hintikka, J. Juoksukangas, M. Honkanen, M. Vippola, A. Lehtovaara, A. Mäntylä, J. Vaara, T. Frondelius, The formation and characterization of fretting-induced degradation layers using quenched and tempered steel, Tribol. Int. 131 (2019) 258–267. https://doi.org/https://doi.org/10.1016/j.triboint.2018.09.012.

[12] J. Juoksukangas, V. Nurmi, J. Hintikka, M. Vippola, A. Lehtovaara, A. Mäntylä, J. Vaara, T. Frondelius, Characterization of cracks formed in large flat-on-flat fretting contact, Int. J. Fatigue. 124 (2019) 361–370. https://doi.org/10.1016/j.ijfatigue.2019.03.004.

[13] S. Fouvry, P. Arnaud, A. Mignot, P. Neubauer, Contact size, frequency and cyclic normal force effects on Ti–6Al–4V fretting wear processes: An approach combining friction power and contact oxygenation, Tribol. Int. 113 (2017) 460–473.

[14] A.M. Kirk, P.H. Shipway, W. Sun, C.J. Bennett, The effect of frequency on both the debris and the development of the tribologically transformed structure during fretting wear of a high strength steel, Wear. 426–427 (2019) 694–703. https://doi.org/10.1016/j.wear.2018.12.035.

[15] S. Baydoun, S. Fouvry, An experimental investigation of adhesive wear extension in fretting interface: Application of the contact oxygenation concept, Tribol. Int. 147 (2020) 106266. https://doi.org/10.1016/J.TRIBOINT.2020.106266.

[16] E. Sauger, S. Fouvry, L. Ponsonnet, P. Kapsa, J.M. Martin, L. Vincent, Tribologically transformed structure in fretting, Wear. 245 (2000) 39–52. https://doi.org/10.1016/S0043-1648(00)00464-6.

[17] I.M. Feng, H.H. Uhlig, Fretting corrosion of mild steel in air and in nitrogen, J. Appl. Mech. 21

(1954) 395–400.

[18] H. Uhlig, Mechanism of fretting corrosion, J. Appl. Mech. 21 (1954) 401–407.

[19] B. van Peteghem, S. Fouvry, J. Petit, Effect of variable normal force and frequency on fretting wear response of Ti–6Al–4V contact, Wear. 271 (2011) 1535–1542. https://doi.org/https://doi.org/10.1016/j.wear.2011.01.060.

[20] A.R. Warmuth, P.H. Shipway, W. Sun, Fretting wear mapping: The influence of contact geometry and frequency on debris formation and ejection for a steel-on-steel pair, Proc. R. Soc. A Math. Phys. Eng. Sci. 471 (2015). https://doi.org/10.1098/rspa.2014.0291.

[21] X. Jin, P.H. Shipway, W. Sun, The role of frictional power dissipation (as a function of frequency) and test temperature on contact temperature and the subsequent wear behaviour in a stainless steel contact in fretting, Wear. 330–331 (2015) 103–111. https://doi.org/10.1016/j.wear.2015.02.022.

[22] A. Dréano, S. Fouvry, G. Guillonneau, A tribo-oxidation abrasive wear model to quantify the wear rate of a cobalt-based alloy subjected to fretting in low-to-medium temperature conditions, Tribol. Int. 125 (2018) 128–140. https://doi.org/10.1016/j.triboint.2018.04.032.

[23] S. Baydoun, S. Fouvry, S. Descartes, P. Arnaud, Fretting wear rate evolution of a flat-on-flat low alloyed steel contact: A weighted friction energy formulation, Wear. 426–427 (2019) 676–693. https://doi.org/https://doi.org/10.1016/j.wear.2018.12.022.

[24] S. Baydoun, P. Arnaud, S. Fouvry, Modelling adhesive wear extension in fretting interfaces: An advection-dispersion-reaction contact oxygenation approach, Tribol. Int. (2020) 106490. https://doi.org/https://doi.org/10.1016/j.triboint.2020.106490.

[25] C. Mary, T. Le Mogne, B. Beaugiraud, B. Vacher, J.M. Martin, S. Fouvry, Tribochemistry of a Ti alloy under fretting in air: Evidence of titanium nitride formation, Tribol. Lett. 34 (2009) 211–222. https://doi.org/10.1007/s11249-009-9426-6.

[26] T. Zhu, P.H. Shipway, W. Sun, The dependence of wear rate on wear scar size in fretting; the role of debris (third body) expulsion from the contact, Wear. 440–441 (2019). https://doi.org/10.1016/j.wear.2019.203081.

[27] P.H. Shipway, Time-dependence and exposure-dependence of material removal rates in fretting, Wear. (2021) 203826. https://doi.org/https://doi.org/10.1016/j.wear.2021.203826.

[28] G.H.G. Vaessen, C.P.L. Commissaris, A.W.J. De Gee, Fretting Corrosion of Cu-Ni–Al against Plain Carbon Steel, in: Proc. Inst. Mech. Eng. Conf. Proc., SAGE Publications Sage UK: London, England, 1968: pp. 125–128.

[29] L. Toth, The investigation of the steady stage of steel fretting, Wear. 20 (1972) 277–286. https://doi.org/https://doi.org/10.1016/0043-1648(72)90409-7.

[30] R.B. Waterhouse, Fretting corrosion, Pergamon Press, 1972.

[31] N. Ohmae, T. Tsukizoe, The effect of slip amplitude on fretting, Wear. 27 (1974) 281–294. https://doi.org/https://doi.org/10.1016/0043-1648(74)90114-8.

[32] O. Vingsbo, S. Söderberg, On fretting maps, Wear. 126 (1988) 131–147. https://doi.org/10.1016/0043-1648(88)90134-2.

[33] J. Halliday, W. Hirst, The fretting corrosion of mild steel, Proc. R. Soc. A Math. Phys. Eng. Sci. 236 (1956) 411–425.

[34] X. Zhang, C. Zhang, C. Zhu, Slip amplitude effects and microstructural characteristics of surface layers in fretting wear of carbon steel, Wear. 134 (1989) 297–309.

[35] S.R. Pearson, P.H. Shipway, J.O. Abere, R.A.A. Hewitt, The effect of temperature on wear and friction of a high strength steel in fretting, Wear. 303 (2013) 622–631. https://doi.org/10.1016/j.wear.2013.03.048.

[36] E.K. Hayes, P.H. Shipway, Effect of test conditions on the temperature at which a protective debris bed is formed in fretting of a high strength steel, Wear. 376–377 (2017) 1460–1466. https://doi.org/10.1016/j.wear.2017.01.057.

[37] J. Jiang, F.H. Stott, M.M. Stack, The role of triboparticulates in dry sliding wear, Tribol. Int. 31 (1998) 245–256. https://doi.org/10.1016/S0301-679X(98)00027-9.

[38] F. Alkelae, S. Fouvry, Identification of parameters influencing the glaze layer formation and stability at high temperature for a Waspaloy/René125 contact under fretting wear conditions, Wear. 390–391 (2017) 41–48. https://doi.org/10.1016/j.wear.2017.07.008.

[39] R. Rybiak, S. Fouvry, B. Bonnet, Fretting wear of stainless steels under variable temperature conditions: Introduction of a "composite" wear law, Wear. 268 (2010) 413–423. https://doi.org/10.1016/j.wear.2009.08.029.

[40] J.E. Wilson, F.H. Stott, G.C. Wood, Development of wear-protective oxides and their influence on sliding friction, Proc. R. Soc. London, Ser. A Math. Phys. Sci. 369 (1980) 557–574.

[41] F.H. Stott, The role of oxidation in the wear of alloys, Tribol. Int. 31 (1998) 61–71. https://doi.org/10.1016/S0301-679X(98)00008-5.

[42] T. Kayaba, A. Iwabuchi, The fretting wear of 0.45% C steel and austenitic stainless steel from 20 to 650 °C in air, Wear. 74 (1981) 229–245. https://doi.org/https://doi.org/10.1016/0043-1648(81)90165-4.

[43] A.L. Mohd Tobi, J. Ding, S. Pearson, S.B. Leen, P.H. Shipway, The effect of gross sliding fretting wear on stress distributions in thin W-DLC coating systems, Tribol. Int. 43 (2010) 1917–1932. https://doi.org/10.1016/j.triboint.2010.01.018.

[44] S.B. Leen, I.J. Richardson, I.R. McColl, E.J. Williams, T.R. Hyde, Macroscopic fretting variables in a splined coupling under combined torque and axial load, J. Strain Anal. Eng. Des. 36 (2001) 481–497. https://doi.org/10.1243/0309324011514647.

[45] S. Fouvry, T. Liskiewicz, P. Kapsa, S. Hannel, E. Sauger, An energy description of wear mechanisms and its applications to oscillating sliding contacts, Wear. 255 (2003) 287–298. https://doi.org/https://doi.org/10.1016/S0043-1648(03)00117-0.

[46] A.R. Warmuth, The effect of contact geometry and frequency on dry and lubricated fretting wear, University of Nottingham, 2014.

[47] J.D. Lemm, A.R. Warmuth, S.R. Pearson, P.H. Shipway, The influence of surface hardness on the fretting wear of steel pairs—Its role in debris retention in the contact, Tribol. Int. 81 (2015) 258–266. https://doi.org/https://doi.org/10.1016/j.triboint.2014.09.003.

[48] A.M. Kirk, P.H. Shipway, W. Sun, C.J. Bennett, Debris development in fretting contacts – Debris particles and debris beds, Tribol. Int. (2019). https://doi.org/10.1016/j.triboint.2019.01.051.